Lawrence Berkeley National Laboratory
Recent Work

Title

MOLECULAR BEAM SOURCES FABRICATED FROM MULTICHANNEL ARRAYS: V MEASUREMENT OF THE SPEED DISTRIBUTION

Permalink

https://escholarship.org/uc/item/796256g9

Authors

Siekhaus, W.J.
Jones, R.H.
Olander, D.R.

Publication Date

1970-05-01

MOLECULAR BEAM SOURCES
FABRICATED FROM MULTICHANNEL ARRAYS:
V. MEASUREMENT OF THE SPEED DISTRIBUTION

W. J. Siekhaus, R. H. Jones, and D. R. Olander

May 1970

LAWRENCE RADIATION LABORATORY
UNIVERSITY of CALIFORNIA BERKELEY

DISCLAIMER

MOLECULAR BEAM SOURCES FABRICATED FROM
MULTICHANNEL ARRAYS: V MEASUREMENT OF THE SPEED DISTRIBUTION

by W. J. Siekhaus, R. H. Jones and D. R. Olander

Inorganic Materials Research Division of the
Lawrence Radiation Laboratory and
the Department of Nuclear Engineering
University of California, Berkeley, California 94720

ABSTRACT

A technique for measuring the speed distribution of molecular beams which uses symmetric modulation and phase sensitive detection is described. Corrections for system errors on experiments of this type are developed and verified. In addition to the expected 1/v dependence of the ionizer, the extraction efficiency of the quadrupole mass spectrometer ionizer is shown to depend on the velocity of the molecules before ionization. The prediction of 5.5% energy enhancement of beams from channel sources operated at pressures well above the free-molecule flow limit has been verified.

I. INTRODUCTION

Molecular beams generated by channel sources are used in many laboratories to investigate the physical-chemical interactions (reaction or scattering) between the beam and a solid surface or another gas. To utilize these sources efficiently and to interpret correctly the results of beam-surface or beam-beam interaction measurements, the distribution of the molecular beam both in velocity and in space must be understood. The total flow rates and angular distributions from a variety of beam sources have been investigated in this laboratory (1). A theoretical prediction of the speed distribution in the centerline beam was also developed (2). The subject of the present report is the measurement of the speed distribution.

The technique used here to measure the speed distribution in the molecular beam differs in several significant ways from the methods conventionally employed for such studies. The new technique appears to have some advantages over the older methods, and in addition, requires only the equipment and operating techniques normally used for surface reaction or scattering studies.

The oldest and most straightforward method of measuring the velocity distribution of a molecular beam is by means of a velocity selector, which is a series of rotating slotted disks. The technique is of limited utility in systems where

short flight paths are desired or for beams of non-condensible gases.

A technique which has become popular for measuring the velocity distribution of aerodynamic beams is the time-of-flight method. Here the beam is periodically gated "on" and the number of beam molecules arriving at a detector downstream is recorded.

The time between pulses is generally long enough to prevent the signals from adjacent pulses from overlapping. If the pulse "on" time Δt is small compared to the average transit time, the pulse can be regarded as a delta function and interpretation of the time-of-arrival signal is greatly simplified. Typically, Δt is ∿1% of the time between pulses (3), and as a result, only a small fraction of the available beam is utilized.

If the chopper is open for a time comparable to the flight time of the molecules, the signal is a convolution of the velocity distribution and the gating function (4,5), and inversion of the data to yield the velocity distribution is difficult. Analytic inversion is possible only for simple gating functions, such as an isosceles triangle (5). Very accurate data are required since the second derivative of the time-of-arrival curve is needed. Generally, only the lower moments of the velocity distribution can be determined accurately. Alternatively, a velocity distribution

function containing adjustable parameters can be utilized with the known gating function to achieve a best fit to the time-of-arrival curve (6). While this procedure is well adapted to aerodynamic beams, where a drifting Maxwellian distribution is theoretically expected, it is less useful in situations where the form of the distribution function is not known a priori.

In the method used here, the molecular beam is symmetrically modulated, which means that 50% of the available beam is utilized. The amplitude and phase of the signal from a detector located downstream of the chopper are measured with a phase sensitive lock-in amplifier over a wide range of chopping frequencies. These data represent a Fourier transform of the velocity distribution. Because the results do not depend on the gating function of the chopper, inversion of the measurements obtained in frequency space to yield the velocity distribution is straightforward.

II. THEORY OF THE TECHNIQUE

Consider a steady molecular beam emanating from a source into a vacuum chamber containing a detector through which the beam can pass unobstructed. Let the total number density of beam molecules at the detector location be n_{ss}, which is assumed to be constant over the sensitive volume of the ionizer. Now interpose a beam modulator or chopper between the source and the detector. If the periodic function g(t) denotes the fraction of the total beam cross sectional area exposed by the chopper at time t, the instantaneous density of beam molecules with reduced speeds between z and z + dz in the detector is:

$$n(z,t)dz = n_{ss}g(t - \ell/\alpha z)f(z)dz \qquad (1)$$

where f(z) is the number density speed distribution along the axis
of the molecular beam and ℓ is the distance between the chopper and
the detector. Molecular speeds have been expressed in terms of the
reduced speed, $z = v/\alpha$ where $\alpha = (2kT/m)^{1/2}$ is the most probable
speed of a Maxwellian gas at the temperature of the source. $\ell/\alpha z$ is
the transit time of molecules of reduced speed z.

The detector considered here is a quadrupole mass spectrometer
with a flow-through ionizer in which an electron beam intersects the
molecular beam. If the electron current density at a location $\underline{r}$ in
the ionizer is denoted by $I_e(\underline{r})$, the rate of production of ions from
neutrals originally in the speed range z to z + dz in the volume
element d^3r at $\underline{r}$ is:

$$R^+(\underline{r},z,t)d^3r\ dz = \sigma_e I_e(\underline{r})n(z,t)d^3r\ dz \tag{2}$$

where σ_e is the ionization cross section.

The probability of extraction and transmission of an ion once it
has been created may depend upon the speed of the neutral molecule
from which the ion was formed and on the location of the ionization
event. A quantity $p(\underline{r},z)$ is defined as the probability that a
molecule of reduced speed z which has undergone ionization at location
$\underline{r}$ in the ionizer succeeds in passing through the mass spectrometer and
registering as an output signal. This probability may also depend
upon the direction in which the molecule is traveling at the time of
ionization. This possibility is not considered here, since the
molecular beam in our experiments traversed the ionizer in a fixed
direction. The average probability of ion extraction and transmission

for molecules of reduced speed z in the ionization volume is:

$$B_V(z) = \frac{\int_V I_e(\underline{r}) p(\underline{r}, z) d^3 r}{\int_V I_e(\underline{r}) d^3 r} \tag{3}$$

where V denotes the volume in which the molecular and electron beams overlap. The subscript V on the average probability indicates that unless $p(\underline{r}, z)$ is separable in $\underline{r}$ and z, the z-dependence of the extraction-transmission efficiency as well as its magnitude depends upon the region in which ionization occurs.

The probability that any ion is detected is:

$$B_V = \int_0^\infty B_V(z) f(z) \, dz$$

which is the usual ion extraction and transmission efficiency of the detector. The subscript V again emphasizes that this efficiency depends upon the position of the ionization region.

Our experiments were not capable of measuring the magnitude of B_V or $B_V(z)$. We could only determine quantitatively the dependence of the probability in Eq(3) upon molecular speed, and qualitatively, the dependence of this functional relationship upon the position of the ionization volume within the ionizer. The function describing the dependence of $B_V(z)$ upon z is termed the "detector bias function". For clarity of presentation, the subscript V will be omitted, although it should be understood that both the magnitude and z-dependence of the extraction-transmission efficiency depend strongly upon the location of the ionization region.

The detector bias function (both magnitude and z-dependence)

depends upon the voltages applied to the various plates of the ion extraction lens. The effect of electronic settings on the z-dependence was noted in the experiments.

All subsequent signal development steps (production of secondary electrons, electron multiplication and current-to-voltage conversion) are assumed to be independent of the initial speed of the molecule prior to ionization.

An electron multiplier following the mass filter amplifies the current. The output current from the electron multiplier is dropped across a load resistor R_L and presents a voltage at the input of the lock-in amplifier. Stray capacitance across the load resistor makes the load appear as a complex impedance.

The signal voltage entering the lock-in amplifier due to ionization of beam molecules with thermal speeds in z to z + dz at time t can be written as:

$$S(z,t) \ dz = G\mathcal{L}\left\{ \int_V R^+(\underline{r},z,t)p(\underline{r},z)d^3r \right\} dz \qquad (4)$$

where G is the gain of the electron multiplier, and $\mathcal{L}$ is a linear operator which represents the complex impedance of the transmission line. It accounts for the load resistor which transforms the electron multiplier output current into a voltage at the input of the lock-in amplifier and for the stray capacity which integrates this input signal. If there were no stray capacitance, $\mathcal{L}$ would be a real constant. Combining

Eqs. (1)-(4) and integrating over all speeds, the input signal to the lock-in amplifier can be written as:

$$S(t) = \left[G\sigma_e n_{ss} \int_V I_e(\underline{r}) d^3r \right] \times \int_0^\infty g(t - \ell/\alpha z) B(z) f(z) \, dz \qquad (5)$$

The DC component of the gating function does not contribute to the signal because the lock-in input is AC coupled. Therefore, the gating function $g(t)$ may be taken to be an odd periodic function which can be expanded in a Fourier sine series:

$$g(t - \ell/\alpha z) = \sum_{n=1}^\infty \beta_n \sin\left[n\omega_m (t - \ell/\alpha z) \right] \qquad (6)$$

where

$$\beta_n = \frac{\omega_m}{\pi} \int_0^{2\pi/\omega_m} g(t)\sin(n\omega_m t)dt \tag{7}$$

and ω_m is the fundamental frequency of the modulation. When the series expression for $g(t - \ell/\alpha z)$ is substituted into Eq. (5) and the $\mathscr{L}$ operation is brought inside the summation we obtain,

$$S(t) = C \int_0^\infty B(z)f(z) \sum_{n=1}^\infty \beta_n \mathscr{L}\left\{\sin\left[n\omega_m(t - \ell/\alpha z)\right]\right\} dz \tag{8}$$

where the parameters in the square bracket of Eq. (5) have been collected in the constant C.

The $\mathscr{L}$ operation on the bracketed term in Eq. (8) is equivalent to the voltage response of the circuit (composed of the load resistance and stray capacity) to a current excitation $\sin[n\omega_m(t - \ell/\alpha z)]$ and may be written as:

$$\mathscr{L}\left\{\sin\left[n\omega_m(t - \ell/\alpha z)\right]\right\} = |Z(n\omega_m)|\sin\left[n\omega_m(t - \ell/\alpha z) + \phi_Z(n\omega_m)\right]$$
$$\tag{9}$$

where $|Z(n\omega_m)|$ is the magnitude of the transfer impedance of the circuit at the frequency $n\omega_n$ and $\phi_Z(n\omega_m)$ is the phase angle of the transfer impedance.

The signal at the input of the lock-in amplifier is then,

$$S(t) = C \int_0^\infty B(z)f(z) \sum_{n=1}^\infty \beta_n |Z(n\omega_m)| \sin\left[n\omega_m(t - \ell/\alpha z) + \phi_Z(n\omega_m)\right] dz$$

$$(10)$$

The phase sensitive amplifier passes the input signal $S(t)$ through a narrow band amplifier of center frequency ω, then synchronously rectifies this signal in an electronic switch which is controlled by a reference signal. No output is obtained unless the frequency ω is "locked-in" with the modulation frequency ω_m or one of its harmonics, $2\omega_m$, $3\omega_m$, etc. These signal processing steps essentially amount to multiplying the input signal by a reference sinusoid $\sin(\omega t - \phi)$ where ϕ is the angle by which the reference sinusoid lags the reference signal triggering it. The product signal from the synchronous rectifier is averaged over a time sufficient to smooth out fluctuations.

The output signal after passing through the lock-in amplifier may be written as

$$A(\omega, \ell, \phi) = \lim_{T \to \infty} \frac{C}{T} \int_0^T \sin(\omega t - \phi) \int_0^\infty B(z)f(z)$$

$$\sum_{n=1}^\infty \beta_n |Z(n\omega_m)| \sin\left[n\omega_m(t - \ell/\alpha z) + \phi_Z(n\omega_m)\right] dz dt$$

$$(11)$$

If the lock-in amplifier is tuned to the fundamental mode $\omega = \omega_m$, only the n=1 term in the sum contributes and we obtain

$$A(\omega,\ell,\phi) = \lim_{T\to\infty} \frac{C}{T} \int_0^T \int_0^\infty B(z)f(z)\beta_1|Z(\omega)|\frac{1}{2}\left\{\cos\left[\frac{\omega\ell}{\alpha z} - \phi - \phi_Z(\omega)\right]\right.$$

$$\left. - \cos\left[2\omega t - \phi - \frac{\omega\ell}{\alpha z} + \phi_Z(\omega)\right]\right\} dzdt \qquad (12)$$

Integrating over time the second cosine term drops out and we are left with,

$$A(\omega,\ell,\phi) = \frac{1}{2} C\beta_1|Z(\omega)| \int_0^\infty B(z)f(z)\cos\left[\frac{\omega\ell}{\alpha z} - \phi - \phi_Z(\omega)\right]dz \qquad (13)$$

Notice that the result involves the gating function only through its first Fourier coefficient which may be combined with the constant C.

In performing an experiment the phase ϕ is adjusted to give zero output. The phase angle is shifted 90° from the null point and the output signal A and corresponding value of ϕ are recorded. The characteristics of the external circuit, $|Z(\omega)|$ and $\phi_Z(\omega)$, may be determined independently. Their effects are removed before further data reduction by dividing the measured signal amplitude by $|Z(\omega)|$ and adding $\phi_Z(\omega)$ to the measured phase angle.

After correcting for complex impedance, the amplitude in Eq. (13) is normalized by dividing by the amplitude at zero

frequency and the phase is expressed as the shift from the phase angle at zero frequency. (Phase and amplitude at zero frequency are determined by extrapolation - see Sec. IV) The amplitude and phase so determined are denoted by $\mathcal{Q}$ and ϕ; they represent measurements at a phase angle which maximizes the signal amplitude.

The new amplitude and phase depend on ω and ℓ only through their product $\omega\ell$. The dimensionless parameter $X = \omega\ell/\alpha$ is π times the ratio of the transit time of a molecule of the most probable speed, ℓ/α, to the modulation time π/ω. In terms of X, Eq. (13) becomes:

$$\mathcal{Q}(X) = \frac{1}{C'} \int_0^\infty B(z)f(z) \cos\left[X/z - \phi(X)\right] dz \qquad (14)$$

where C' represents the integral of Eq. (14) when X=0. The zero output at each value of X at a phase angle of $(\phi + 90°)$ is expressed as:

$$0 = \int_0^\infty B(z)f(z) \cos\left\{X/z - \left[\phi(X) + \pi/2\right]\right\} dz \qquad (15)$$

With the substitution $y = 1/z$, Eq. (14) is seen to be the complete Fourier integral transform of the function $B(y)f(y)/y^2$ with respect to the transform variable X. Fourier inversion and resubstitution of $z = 1/y$ yields:

$$z^2 B(z)f(z) = \frac{2}{\pi} C' \int_0^\infty \mathcal{Q}(X) \cos\left[X/z - \phi(X)\right] dX \qquad (16)$$

The normalized distribution function is given by:

$$f(z) = \frac{\dfrac{1}{z^2 B(z)} \displaystyle\int_0^\infty \mathcal{Q}(X)\cos\left[X/z - \Phi(X)\right]dX}{\displaystyle\int_0^\infty \frac{dz}{z^2 B(z)} \int_0^\infty \mathcal{Q}(X)\cos\left[X/z - \Phi(X)\right]dX} \qquad (17)$$

Thus the speed distribution can be determined by integration of the phase and amplitude data over all frequencies (or X).

The average translational energy of the beam molecules is of particular interest in molecular beam experiments. The ratio of the energy of the beam molecules relative to that of a Maxwellian beam is given by Eq. (19) of reference 2. The beam energy ratio can be determined from phase and amplitude data by:

$$\frac{\overline{\epsilon}}{\epsilon_M} = \frac{\displaystyle\int_0^\infty dz\, \frac{z}{B(z)} \int_0^\infty \mathcal{Q}(X)\cos\left[\frac{X}{z} - \Phi(X)\right]dX}{2\displaystyle\int_0^\infty \frac{dz}{z B(z)} \int_0^\infty \mathcal{Q}(X)\cos\left[\frac{X}{z} - \Phi(X)\right]dX} \qquad (18)$$

III. EQUIPMENT

The experiment is designed to perform three functions:
to generate a molecular beam of constant intensity; to modulate
it; and, at a point downstream, to detect the amplitude and phase
of the density variations introduced by the modulation.

The experiment is housed in the vacuum system shown
in Fig. 1. A 1 mm diameter hole in the dividing partition
between the source chamber and the main chamber serves as
the beam collimator. The source chamber is pumped by a
liquid nitrogen trapped 500 lit/sec oil diffusion pump, which maintains
a vacuum of 2×10^{-5} torr when the strongest beam is generated. The
main chamber is the interior of a 1200 lit/sec ion pump operating at
3×10^{-8} torr for strong beams (provided that the chopper in this
chamber is not operated). These pressures are sufficiently low so
that collisions between beam molecules and the background gas are
negligible.

The beam source is a single capillary 0.48 cm in length
and 0.038 cm diameter drilled in a brass plug mounted in the
end of a 1/2 inch diameter brass tube. This source
has been previously tested for angular emission and total
leak rate.[1] Although the single capillary is not as
efficient a source as a multichannel array, the capillary
was chosen for these experiments because the geometry is
accurately known and the possibility of interference between
many channels is avoided.

For the present study an ultra clean gas inlet system

is not necessary. Copper or nylon tubing is used for interconnections and joints are made with viton gaskets. Source pressure is measured on a 0.1 - 20 torr Wallace-Tiernan gauge, and on a 0.01 micron - 10 torr (three range) McLeod gauge trapped with dry ice and acetone. Gas flow is regulated by a Granville Phillips variable leak.

Two beam choppers labelled as nos. 1 and 2 in Fig. 1 are provided in order to vary the flight path. No. 1 is close to the source in the source chamber (molecular flight path, chopper-to-detector = 38.2 cm) and no. 2 is close to the detector in the main chamber (molecular flight path, chopper-to-detector = 2.4 cm). The beam choppers are driven by Globe synchronous motors. The motors are used as received with no change of lubricants, but are mounted in water cooled blocks.
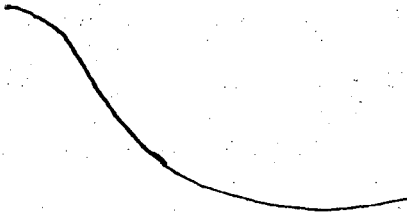
The motors have a design driving speed of 8000 rpm but have operated smoothly from 100 - 14,000 rpm. Some care must be used at low speeds to provide just sufficient driving power to sustain rotation or uneven motion occurs.

The synchronous motors used here require two power sources 90° out of phase. Typically, these small motors are driven by an audio test oscillator through an audio power amplifier. Satisfactory operation at a fixed speed can be achieved by applying power to one winding directly and to the other winding through a phasing capacitor. A more convenient technique is to use two amplifiers each supplying one winding, phase shifting being done before power amplification. (The audio oscillator, a Hewlett Packard model 203A Function Generator, provides two sine wave outputs with variable phase relation.) This technique has the advantage of permitting rapid speed changes and delivers substantially smoother power to the motor; it also allows a reduction in driving power which minimizes motor heating. By applying equal power to both motor windings chopper flutter is reduced. Dynaco Mark III audio amplifiers (60 watts each) were used. An oscilloscope connected across each motor winding to show the 90° Lisajous circle pattern is a convenience to show proper phasing and to indicate overloads.

In other modulated beam systems, a reference signal to use with a lock-in amplifier is usually provided by a photocell-light beam system in the vacuum chamber near the chopper wheel.[7] The compact design of our vacuum system makes such an arrangement impractical. In order to provide a reference signal, the "position" of the rotating wheel is observed with a strobe light (General Radio 1531AB)

synchronized with the motor power and provided with variable
delay by two Data Pulse 101 pulse generators connected in
series. Under some driving conditions, the chopper viewed by
the synchronized strobe appears to "walk" away from the reference
position or to oscillate about it. These indications of marginal
operation of the synchronous drive system are easily observed with
the strobe technique and may be immediately corrected by individually
adjusting power to each motor winding (provided the bearings are
still sound).

The time delay between the
synchronizing pulse and the light output was measured and found
to be about 4×10^{-6} sec. The strobe reference "position" is
viewed through a 12 power cathetometer comparing a blade edge to a line
scratched on the vacuum chamber wall. Reference resettability
is better than 1° phase.

Chopper wheels are 3" in diameter with slots milled
into the edges to provide equal beam "on" and "off" times.
The wheels are checked for static balance by supporting
them at the hub on a conical pivot. Heavy sides are thinned
on the faces by hand grinding. The balancing test can
detect an imbalance of about 1 milligram on the edge.

In order to eliminate pickup of motor hum in the output signal,
the number of slots on the chopper blade was chosen to give a beam
modulation frequency twice that of the motor drive. The motor drive
frequency is then doubled in a full wave bridge to provide a

reference signal at the modulation frequency.

The detector is an Electronics Associates Inc. quadrupole mass spectrometer. A sketch of the spectrometer with typical ionizer operating voltages is shown in Fig. 2. The detector is of the through-flow variety. The neutral beam entering the ionizer is defined by a collimator opening slightly smaller than the open area of the ionizer. The electron beam intersects the neutral beam at right angles. Those molecules which are not ionized while traversing the electrons pass into the main chamber

without scattering from components of the ionizer. A fraction of the ions created are extracted and drawn into the quadrupole mass filter whose axis is orthogonal to both the neutral beam and the electron beam. Ions successfully passing the mass filter strike the first dynode of an electron multiplier. The signal from the electron multiplier can be approximated by the output of an ideal current source proportional to the number of ions striking the first dynode.

The output of the electron multiplier is fed to a model HR-8 Lock-in Amplifier (Princeton Applied Research Corporation). A negative pulse from the delay generator is used for a reference signal and the lock-in amplifier was operated in the automatic mode. Main tuning is adjusted to match the negative spike to the zero crossover of the sinusoidal reference signal produced in the lock-in amplifier. The lock-in amplifier is calibrated point-by-point at each frequency as data are taken. This calibration allows correction for amplitude nonlinearities and the small phase differences between signal and reference channels. Because the frequency trim control is not adjusted at each frequency, corrections of 5% in amplitude and $\pm 8°$ in phase are encountered in the range 10 - 1400 Hz. A United Systems Corporation Z-200-B digital voltmeter is used for signal readout. The type "A" preamplifier is operated remotely in differential mode with an input to one channel only. Locating the preamplifier close to the electron multiplier reduces cable capacitance and differential operation reduces

ground loop problems. A small relay operated from batteries is used to switch the preamplifier from the electron multiplier to the calibrator. The calibrator has a low output impedance (50 ohms); therefore cable capacitances are of no consequence for calibration. While the calibration signal is applied to the preamplifier, the electron multiplier output is connected to an oscilloscipe for visual inspection and to assist in spectrometer adjustments. The inter-connections of the detector electronics are summarized in Fig. 3.

IV. EXPERIMENTAL PROCEDURE

For each set of experiments on a particular gas, the mass spectrometer ionizer controls were fixed by maximizing the output signal from a modulated molecular beam. These settings were found to be independent of modulation frequency and were maintained for the entire series of experiments with that gas.

Depending on the desired path length, one of the two choppers shown in Fig. 1 is utilized. The unused chopper is arrested in an open position, so that it does not obstruct the beam. An experiment begins by setting up the desired pressure in the source tube using the variable leak. After waiting about an hour for equilibrium to be established data taking is begun. The amplitude and phase data are taken beginning with a value at 200 Hz.; then a series of points from 10 Hz. through 200 Hz. up to 1400 Hz. and a final check point at 200 Hz. are taken. The time at which each data point is taken is recorded.

Over the range of source pressures investigated

only slight changes in amplitude and phase data were observed. Consequently operating techniques were developed to minimize scatter of the data and systematic errors were carefully appraised experimentally. The error sources associated with each component are listed in parenthesis in Fig. 1 and are described in more detail in Appendix A.

After correction for the various effects discussed in Appendix A, the phase and amplitude are plotted versus frequency in the frequency range from 10 to 250 Hz. Best fitting lines are drawn through the data points and extrapolated to zero frequency. All amplitude values are normalized by dividing by the value of amplitude at zero frequency.

Absolute zero in phase occurs when the trailing edge of a chopper blade is passing the center of the beam. The reference line viewed under strobe flash does not correspond to this position but represents a fixed value of zero shift. The best value of measured "phase at zero frequency" is obtained by extrapolating several sets of phase data to zero frequency. This zero shift is then applied to correct all phase data, since at low frequencies the phase of all signals approaches the absolute zero of phase.

V.   RESULTS

The Detector Bias Function

If the speed distribution function f(z) and the detector bias function B(z) are known, the amplitude and phase of the

signal as a function of frequency is given by Eqs. (14) and (15).
For a particular X, Φ is determined (to within a constant $2\pi n$)
by Eq. (15) and α is then fixed by Eq. (14). The parameter
X may be eliminated between the two equations to yield a
relation between α and Φ. Harrison, Hummer, and Fite[8]
have determined the amplitude-frequency and phase-frequency
relationships for a constant detector bias function (B(z) =
constant) and a Maxwellian speed distribution $\left(f(z) \sim z^2 e^{-z^2} \right)$.
Their results are expressed as amplitude and phase as functions
of the parameter X. Eliminating this parameter between the
two equations yields a universal amplitude-phase relationship
which is independent of the chopper-to-detector distance,
source temperature, and the molecular weight of the gas.

In Ref. 2, it was shown that completely free molecule
flow and hence a Maxwellian speed distribution is attained when
the Knudsen number (ratio of mean free path in the source
reservoir to channel length) is $\gtrsim 10$. The amplitude-phase
data for two low pressure experiments, oxygen at 1.4 microns
source pressure (Kn = 9.1) and xenon at 0.75 microns (Kn = 9.4),
are plotted in Fig. 4 along with the theoretical curve for a
Maxwellian gas taken from the calculations of Ref. 8. The
results for the two gases are identical within experimental
error, but both lie as much as 20% above the theoretical curve.
This discrepancy is an order of magnitude greater than the
precision of the amplitude measurements. Since the very low
source pressures used in these experiments assured a Maxwellian

speed distribution, the discrepancy in Fig. 4 is ascribed to the detector bias function.

If the disagreement between theory and experiment evident in Fig. 4 is due to a speed sensitive extraction and transmission efficiency of the quadrupole mass spectrometer, the detector bias function should be a function of the position of the neutral beam within the ionizer cage as well as of the speed of the neutral molecules. An experiment was performed to demonstrate that the experimental points of Fig. 4 can be shifted simply by directing the molecular beam to a different portion of the ionizer.

The upper portion of the ionizer was blocked off by arresting chopper No. 2 in the closed position and raising it slightly to allow the neutral beam to pass through the bottom 1/8 of the ionizer. Whereas the amplitude-phase data with a completely open ionizer fell above the theoretical curve, the data from the experiment at the same source pressure and with the same gas fell distinctly below the theoretical curve at low phase angles. Fig. 5 compares the data from these two experiments. These results clearly demonstrate the significant effect of location of the ionization events upon the efficiency of ion extraction and transmission in the mass spectrometer detector.

In another experiment, the voltages on the various plates of the ionizer were not optimized. The amplitude-

phase data were quite different from those obtained under other-
wise identical conditions but with ionizer voltages adjusted
for optimum signal strength.

The detector bias function was determined experimentally
from the xenon data of Fig. 4. The amplitude-frequency and
phase-frequency data were integrated according to Eq. (16).
A computer program fitted a parabola to each trio of
data points and performed the integration with respect to
X numerically until all data points were exhausted. This
distribution was divided by the normalized Maxwellian
speed distribution to yield a quantity proportional to the detector
bias function. The results for the 0.75 micron xenon experiment
is shown in Fig. 6 in which the detector bias function is
plotted as a function of reduced speed, $z = v/\alpha$. The scatter
of the data at low velocities is due to rapid oscillation of the
integrand in Eq. (16) at large values of the X/z term which
leads to difficulties in numerical integration. The detector
bias function from the low pressure oxygen experiment
was the same as that shown in Fig. 6 for xenon. The independence
of the detector bias function on the mass of the gas molecules
when expressed as a function of z   suggests that the
transmission and extraction efficiencies of the detector are
energy rather than speed sensitive (the reduced speed v/α is
equal to the square root of the relative energy $(E/E_o)^{1/2}$,
where E_o is the most probable energy of the distribution).
Fig. 6 also shows that when the ionizer voltages have been

adjusted to give the maximum signal, the maximum in the bias function coincides with the maximum in the distribution function ($z = 1$).

To understand why the extraction and transmission efficiencies of the detector might be maximized at a particular translational energy, consider the path of a molecule in the beam passing through the detector (Fig. 2). The molecule enters the ionizer cage with a particular energy in the thermal range and is ionized with a probability inversely proportional to its speed (or proportional to its residence time in the ionizing region). This behavior renders the detector density sensitive. Once the molecule is ionized, it is subjected to the forces of the electric fields in the ionizer cage. Although the geometry and variety of voltages applied to the many components of the ionizer assembly precludes quantitative computation of the fields inside the cage, two important contributions can be considered qualitatively.

A force due to the electrostatic field between the filament and the electron collector acts on the ion in the direction parallel to the electron beam. The extent to which the ion is deflected towards the filament and away from the ion extractor hole is inversely proportional to its energy. Consequently, low speed molecules are more likely to be diverted from a trajectory which would ultimately result in detection than fast ones.

The force due to the electric field set up by the focus

electrode reaches up through the ion extraction hole and pulls ions towards the quadrupole structure. The probability that an ion is bent by 90° in this extraction process and transported into the quadrupole structure within the acceptance angle of the latter is inversely proportional to the ion energy. This effect renders extraction and transmission of ions with large initial thermal energies in the direction of the neutral beam more difficult than collection of slow molecules.

These two effects suggest that extraction is inefficient for both slow and fast molecules which have been ionized. Optimizing the ionizer controls to obtain the maximum signal apparently varies the two fields described above in a fashion such that the molecule with the most probable energy is also the one most likely to be detected. In a gross sense, the optimization process can be viewed as translation of the detector bias function along the z axis in Fig. 6. The optimum position is at $z = 1$ because this is the speed region containing the largest number of molecules.

Because the ion trajectories under the influence of the electrostatic fields depend upon ion energy, the detector bias function should be a function of the energy of the ion at the instant of ionization (or the reduced speed z) rather than its absolute speed. Comparison of the amplitude-phase data for oxygen and xenon in Fig. 4 indicates that this expectation is fulfilled.

Because of the existence of a detector bias function, the simple method of correcting mass spectrometer output signals for beam temperature by weighting the signals with the square root of the temperature[7] is not valid. The appropriate correction is discussed in Appendix B.

Effect of Source Pressure on the Speed Distribution

Experiments were performed with xenon and oxygen beams over a range of source pressures corresponding to Knudsen numbers (based on channel length) from 10 to 0.02. This range corresponds to 0.75 to 370 microns source pressure for xenon, and 1.4 to 660 microns source pressure for oxygen. Knudsen numbers greater than 10 could not be investigated because the beams were too weak to assure amplitude and phase data of the quality needed for speed distribution studies. Beams characterized by Knudsen numbers smaller than 0.02 were so strong that the electron multiplier degradation was too rapid to obtain reliable data. Nonetheless, the 500-fold source pressure range was sufficient to encompass the transition from Maxwellian to saturated spectra discussed in the previous paper.

The beam was modulated by the chopper in the source chamber which provided a 38.2 cm flight path for the beam molecules. This path length and the maximum modulation frequency of 1400 Hz. was sufficient to reduce the amplitude of the xenon beam to 2.5% of its zero frequency value; the oxygen beam was reduced to 15% of its zero frequency value.

Amplitude degradations due to molecular transit of this magnitude are required to permit the inversion process to be accomplished with reasonable accuracy. The main chamber chopper was arrested in the open position in these experiments.

The lowest pressure xenon experiment was assumed to represent a Maxwellian beam and was used to determine the detector bias function. The data from the remaining eleven experiments were inverted by Eq. (17), using the detector bias function shown on Fig. 6. Figs. 7 and 8 show the amplitude and phase data (after correction for the effects discussed in Appendix A and normalization to unit amplitude and zero phase at zero chopping frequency) for the two xenon beam experiments at the source pressure extremes of the range covered. Figs. 9 and 10 show similar plots for oxygen. These plots illustrate the small differences from which information concerning the effect of source pressure on the spectrum must be extracted.

Experimental and theoretical speed distributions are compared in Fig. 11. The curves are reproductions of Fig. 2 of the preceeding paper, and represent Maxwellian and fully saturated spectra. The measured speed distribution for the xenon experiment at a Knudsen number of 0.02 is in good agreement with the theoretical prediction for the fully saturated spectrum. The theoretical and experimental distributions match quite well around the maximum; the increase in the position

of the maximum compared to a Maxwellian distribution is in

excellent accord with the collision model discussed in the

previous paper. The experimental points at low speeds

($z < 0.5$) exhibit considerable scatter. The theoretical

curve for the fully saturated spectrum is $\sim 10\%$ lower than

the measured distribution at high speeds. These data are

not sufficiently precise to ascribe this discrepancy to an

inadequacy in the model used to generate the theoretical

curve.

The ratio of the average translational energy of the beam

molecules to that for a Maxwellian beam is a useful quantity

for characterizing the entire speed distribution. This quantity

is determined from the data by use of Eq. (17) and compared in

Fig. 12 to the predictions of the collision model developed

in the preceeding paper. Because of the fluctuations

introduced by the inversion technique, the points show

considerable scatter about the theoretical curve.

However, the

agreement is considered adequate in view of the small range over which the beam energy ratio changes and the many corrections required before the data can be inverted. The deviations of the data from the theoretical curve are never more than 4%, which is small compared to the 25 or 75% changes in the beam energy ratio which would be expected for a fully expanded nozzle beam. Within the scatter of the data, diatomic oxygen and monatomic xenon yield similar spectrum hardening parameters, which is expected for the collision model on which the theory is based, but which would not be so if aerodynamic effects were significant. Although the data do not verify the existence of the plateau at low Knudsen numbers, the ∿5 1/2% increase in beam energy ratio at high source pressures predicted by the theory is consistent with the measurements.

VI. <u>CONCLUSIONS</u>

1) The results suggest that lock-in amplification of symmetrically modulated molecular beams may be a useful tool for measuring the speed distribution in molecular beams.

2) Both the average energy of the beam and the speed distribution measured by this technique are consistent with predictions of the collision model developed in the previous paper. The hardening of molecular beams from channel sources operated just above the free molecule limit is small compared to the substantial increase of beam energy obtainable from

nozzle beams. The difference between the beams from channel sources such as those considered in this series of papers and the ideal Maxwellian beam may be significant enough to warrant consideration in some beam-beam or beam-surface interaction studies.

3) The quadrupole mass spectrometer, which is a popular detector for studies of this nature, is not a purely density-sensitive device. Because of tuning the ionizer for maximum signal, the extraction and transmission of ions formed from molecules around the most probable energy of the distribution is favored. The detector bias function which describes this phenomenon is sensitive to the location of the molecular beam in the ionizer and to the voltage settings on the ionizer lens. The bias function undoubtedly varies from one detector to another. The effect of the bias function must be considered when comparing mass spectrometer output signals from beams of different temperatures.

APPENDIX A

SOURCES OF ERROR AND CORRECTIONS

Sources of Error

A. Source Pressure Fluctuations

The pressure in the source generating the beam is held constant to better than 1% over the duration of an experiment. This small long term drift in the beam intensity is included in the correction for electron multiplier gain decay discussed later.

B. Flutter of the Chopper

Although the synchronous motor is commonly regarded as a smoothly rotating device, its motion is derived from a series of cooperating impulses smoothed by the inertia of the rotor and load. Since rotational energy decreases as the square of the frequency of rotation, the angular moment applied (in impulses) to the wheel should be reduced correspondingly to assure that uniform rotation is obtained. Because of the low power applied at low frequencies, large oscillations around the synchronous position can occur. Data were taken only if these oscillations were less than 1° phase.

C. Background Pressure Modulation in the Main Chamber

The pulsed beam entering the main chamber may introduce modulation of the background pressure. An experiment was performed to ascertain that the measured density variations were due to modulation of the directed molecular beam rather than pressure oscillations or beam reflections. Chopper

No. 2 was arrested in a position such that the direct beam was prevented from entering the ionizer cage. An attempt to measure a modulated signal from a strong xenon beam at 10, 700 and 1400 Hz was made. Less than one microvolt of modulated "background" signal was detected at a primary modulated beam signal of one volt. This experiment eliminates background modulation as a significant source of experimental error.

Corrections

The errors introduced in the detection and measuring system which could not be eliminated by careful experimentation alone had to be accounted for by application of correction factors. For this discussion the detection and measuring system is divided into four elements. The error introduced in each of these is listed in parentheses in Fig. 1 under the component involved.

A. Lock-in Amplifier Response

The lock-in amplifier amplifies the signal received from the transmission line and determines its amplitude and the phase with respect to the modulation reference signal. Variations in amplifier gain and phase are corrected by measuring the amplitude and phase response to a full scale-zero phase calibration signal at each frequency.

B. Electron Multiplier Gain Decay

Ideally, the electron multiplier converts the ion current into an electron current and increases the number of charge carriers by a fixed factor. In practice, the gain of the

electron multiplier is not constant. Signal amplitude measurements with a steady modulated beam always exhibit a gradual decrease with time. This decrease is most severe with strong beams, being as large as 15%/hour with output signal of 1 microampere. This degredation in gain is believed to be due to a decrease in the secondary electron emission coefficient of the first dynode because of the implantation of ions (Xe^+ or O_2^+). No long term ill effects of dynode degredation have been observed; the electron multiplier seems to recuperate while idle overnight. Apparently the implanted ions diffuse out of the dynode in ~ 12 hours.

During the course of an experiment, the signal at 200 Hz. modulation was measured several times and plotted as a function of time. From this plot the effective system gain at any time during the experiment could be determined and applied as a correction to the other measurements. Besides the decrease in the gain of the electron multiplier, other phenomena affecting signal amplitude over a similar time period (e.g., change in source pressure, change in efficiency of the ionizer are also included in this correction.)

C. Complex Impedance Correction

Because the transmission line and other stray capacitance present a complex impedance to the current output from the electron multiplier, the amplitude and phase must be corrected for this effect. Correction for capacitance effects by a complex transfer impedance was based on the circuit model

shown in Fig. 13. The electron multiplier is assumed to be an ideal current source, I.

The shunt capacitance C represents the distributed capacity of connectors, preamplifier, and electron multiplier. The value of C was measured on an L-C meter (Tektronix Type 130) to be on the order of 60 picofarads. The load resistor, R_L, provides a DC return path for the signal. Its value is chosen so that the signal voltage drop across it is small compared to the voltage drop between the dynodes of the electron multiplier. If the last dynode is allowed to float the gain of the electron multiplier is decreased at a rate dependent upon the beam strength. It was convenient to use a load resistor equal to that of the monitor oscilloscope (1 Megohm); then the same D.C. level was maintained on the last dynode when connected to either the oscilloscope or the lock-in amplifier.

Components c and r are the input coupling capacitor and grid resistor of the preamplifier stage of the lock-in detector. The lock-in amplifier responds to a voltage S at its input, where S is given by Eq. (5). According to Fig. 13, the complex transfer impedance is:

$$\frac{1}{Z(\omega)} = \frac{1}{R_L} + i\omega C + \frac{1}{r + 1/i\omega c} \tag{A-1}$$

$|Z(\omega)|$ and $\phi_Z(\omega)$ may be evaluated from this equation.

The reliability of the complex impedance correction was checked by performing three sets of measurements of

amplitude attenuation and phase shift under constant beam
conditions but using different values for R_L (10^5, 10^6 and
5×10^6 ohms). A plot of these uncorrected measurements in
terms of amplitude vs. frequency is shown in Fig. 14. The
corresponding plot with phase ordinate is shown in Fig. 15.
The amplitude and phase values corrected for complex impedance
are shown for the 0.1 and 5 megohm load resistors in Figs.
16 and 17. The circuit model used for correction aligns
the data of the different runs within the experimental
scatter.

To verify that the overall system had a flat frequency
response the following experiment was performed. The
chopper No. 1 was arrested in an open position and the beam
was modulated using Chopper No. 2. Since the distance between
chopper and ionizer was reduced by a factor of 15.8 the parameter
X covered only ∿6% of the range available when the source
chamber chopper was used to modulate the beam. For X values
in the overlapping range of the two choppers, the corrected
amplitude and phase vs. frequency plots should coincide
if the system has a flat frequency response. Because of the
finite length of the ionization region (∿0.5 cm), the main
chamber chopper-to-detector distance cannot be defined
exactly, and therefore it is convenient to plot amplitude
versus phase, thereby eliminating X (see text).

Fig. 18 shows that the corrected data for short and
long beam path length experiments coincide in the range of

phase covered by the short length experiments. In these experiments, frequencies from 0 to 1100 Hz. were used with chopper No. 2 and 0-200 Hz. chopper No. 1. Therefore it can be concluded that the detection system has a flat frequency response after all of the previously discussed corrections have been applied.

APPENDIX B

EFFECT OF BEAM TEMPERATURE ON THE OUTPUT SIGNAL FROM

A QUADRUPOLE MASS SPECTROMETER

Consider for example a detector which has been optimized with a Maxwellian gas at temperature T_o. Suppose a steady Maxwellian beam of intensity I_o molecules/cm^2-sec at a temperature T_o passes through the detector. The D.C. signal is:

$$S_o \sim \frac{I_o}{\alpha_o} \int_0^\infty B(z) f_M(z) \, dz \qquad (B-1)$$

where the number density in the beam has been written as $I_o/(2\alpha_o/\sqrt{\pi})$. α_o is the most probable speed at T_o, and $f_M(z) \sim z^2 e^{-z^2}$ (Maxwellian distribution).

For a Maxwellian beam at a temperature $T > T_o$ and intensity I, the signal is given by Eq. (B-1) with the subscript o removed. However, since the detector bias function has been determined by optimization at T_o and is unaffected by beam temperature, the argument of B in Eq. (B-1) must be written as $z\alpha/\alpha_o$. The ratio between signals and beam intensities at the two temperatures is:

$$\frac{I/I_o}{S/S_o} = \left(\frac{T}{T_o}\right)^{1/2} \frac{\int_0^\infty B(z) f_M(z) \, dz}{\int_0^\infty B(z\sqrt{T/T_o}) f(z) \, dz} \qquad (B-2)$$

The detector bias function of Fig. 6 does not have a simple analytical representation. However, a simple functional form which qualitatively possesses the essential features of the curve of Fig. 6 is:

$$B(z) \sim z e^{-\frac{1}{2} z^2} \qquad (B-3)$$

Inserting the Maxwellian speed distribution and Eq. (B-3) into Eq. (B-2) yields:

$$\frac{I/I_o}{S/S_o} = \left(\frac{2}{3} + \frac{1}{3} \frac{T}{T_o} \right)^2 \qquad (B-4)$$

By comparison, the usual correction for an ideal density sensitive detector $(B(z) = \text{constant})$ is:

$$\frac{I/I_o}{S/S_o} = \left(\frac{T}{T_o} \right)^{1/2} \qquad (B-5)$$

For a beam four times greater in absolute temperature than the temperature at which the detector was optimized, the ratio of intensities to signals for an ideal density sensitive detector is 2 while for the detector with the bias function of Eq. (B-3), the ratio is 4. A 100% error in relating signal to beam intensity is introduced by neglecting to account for the non-ideality of the detector. The more rapid drop in signal for hot beams in the non-ideal detector than in the purely density sensitive instrument is due to the fact

that although the bias function is fixed in energy space
(or z-space), the molecular speed distribution is translated
to higher energies as the temperature is increased. The
maximum of the bias function and the molecular distribution
function coincide at T_o (since this is where the detector
was optimized) but the two maxima no longer coincide at
$T \neq T_o$. The factor of two degredation of the signal due
to the mismatch of the detector bias function and the speed
distribution could be reduced by re-optimizing the detector
on the hot beam. However, there is no guarantee that the
optimization process results only in simple translation of
the function $B(z)$ along the z-axis. Reliable inference of
beam intensity changes from mass spectrometer output signals
in the presence of beam temperature variations requires
knowledge of the detector bias function at one temperature.
The correction procedure represented by Eq. (B-2) is of
course necessary for any density sensitive detector of the
electron bombardment type for which extraction efficiency
depends upon the thermal energy of the neutral species before
ionization.

LITERATURE CITATIONS

1. R.H. Jones, V.R. Kruger, and D.R. Olander, J. Appl. Phys., 40, 4641 (1969). (Part I of the series)

2. D.R. Olander, R.H. Jones and W.J. Siekhaus, preceeding paper. (Part IV of this series)

3. J.B. Anderson, and J.B. Fenn, Phys. Fluids, 8, 780 (1965).

4. J.P. Moran, H.Y. Washman, and L. Trilling, in Fundamentals of Gas-Surface Interactions, H. Saltsburg, J.N. Smith, and M. Rogers, Eds. (Academic Press Inc., New York, 1967).

5. P.B. Scott, Ph.D. Thesis, Massachusetts Institute of Technology, (1965).

6. W.E. Amend, Ph.D. Thesis, University of California, Berkeley (1968).

7. R.A. Krakowski and D.R. Olander, J. Chem. Phys. 49, 5027 (1968).

8. H. Harrison, D.G. Hummer, and W.L. Fite, J. Chem. Phys. 41, 2567 (1964).

FIGURE CAPTIONS

Fig. 1.   Schematic diagram of vacuum system

Fig. 2.   Sketch of quadrupole head structure with typical

operating voltages

Fig. 3.   Block diagram of detector electronics

Fig. 4.   Amplitude vs. phase for oxygen and xenon compared

with the theoretical behavior for density sensitive

detector.

Fig. 5.   Amplitude vs. phase for the beam passing through

the entire ionizer or limited to the bottom section only.

Fig. 6.   Experimentally determined detector bias function

$B(z)$

Fig. 7.   Amplitude vs. frequency, low and high pressure

xenon experiments

Fig. 8.   Phase vs. frequency, low and high pressure xenon

experiments

Fig. 9.   Amplitude vs. frequency, low and high pressure

oxygen experiments

Fig. 10.   Phase vs. frequency, low and high pressure oxygen

experiments

Fig. 11.   Experimental and theoretical speed distributions

xenon gas Kn = 0.02 (high pressure)

Fig. 12.   Beam energy ratio as a function of length

Knudsen number for oxygen and xenon gas and theory

Fig. 13.   Circuit model for complex impedance of transmission

line

Pump

Source pressure

$\left(\begin{array}{c}\text{Pressure}\\\text{changes}\end{array}\right)$

Source chamber

Collimator

Chopper 2

Main chamber $\left(\begin{array}{c}\text{pressure}\\\text{oscillations}\end{array}\right)$

Beam flag

Mass spectrometer $\left(\begin{array}{c}\text{detector}\\\text{bias}\end{array}\right)$

Chopper 1 $\left(\begin{array}{c}\text{oscillations,}\\\text{flutter}\end{array}\right)$

Gas reservoir

Electron multiplier (degradation)

(Complex impedence)

Lock-in amplifier

(Frequency response)

XBL6911 – 6160

FARADAY CAGE (+I5V)

ELECTRON COLLECTER (+45V)

FOCUS ELECTRODE (-I20V)

NEUTRAL BEAM

TO READ-OUT ELECTRONICS

ELECTRON MULTIPLIER

ION BEAM

QUADRUPOLE ANALYZER

GROUND

ELECTRON BEAM

IONIZER ASSEMBLY (PIERCE GUN)

TUNGSTEN FILAMENT AND ELECTRON FOCUS -90V WITH RESPECT TO FARADAY CAGE

MU-36636

Fig 2

XBL 6911 - 6159

XBL69II-6136

4

XBL6911-6135

z = v/α

XBL6911- 6163

6
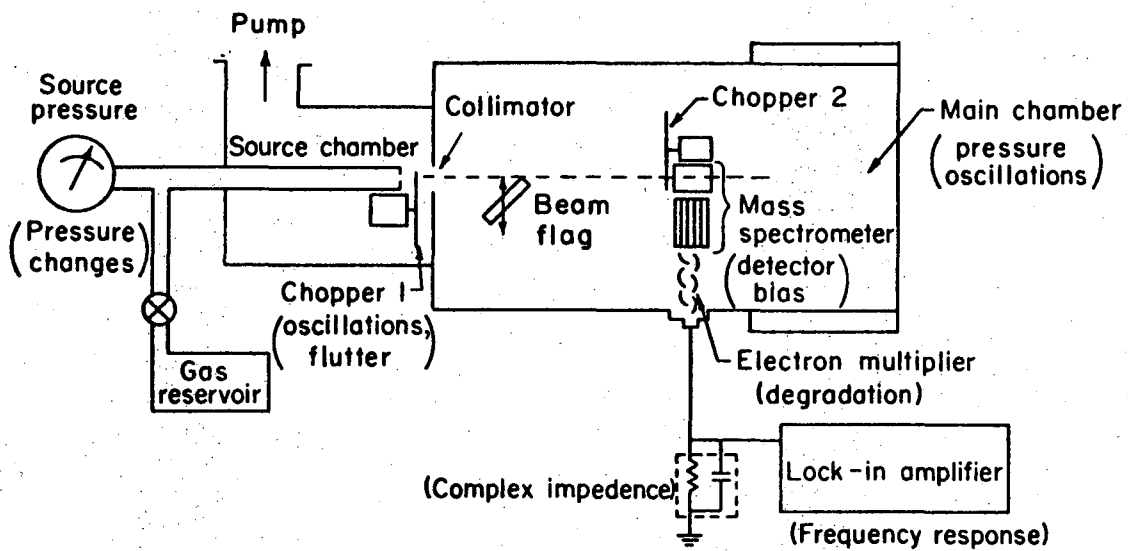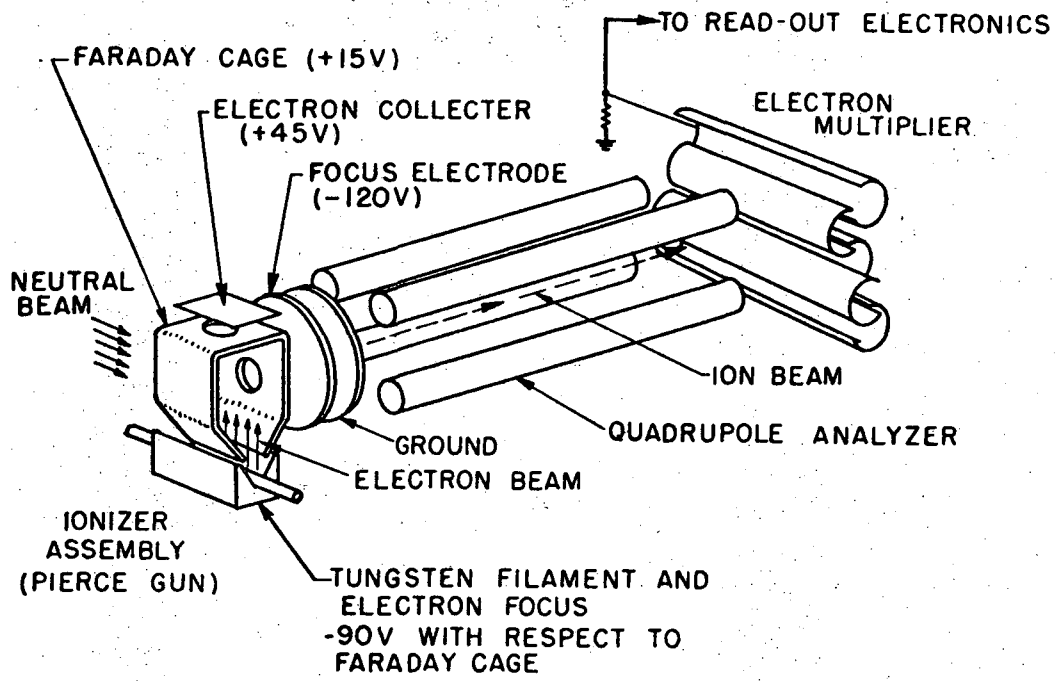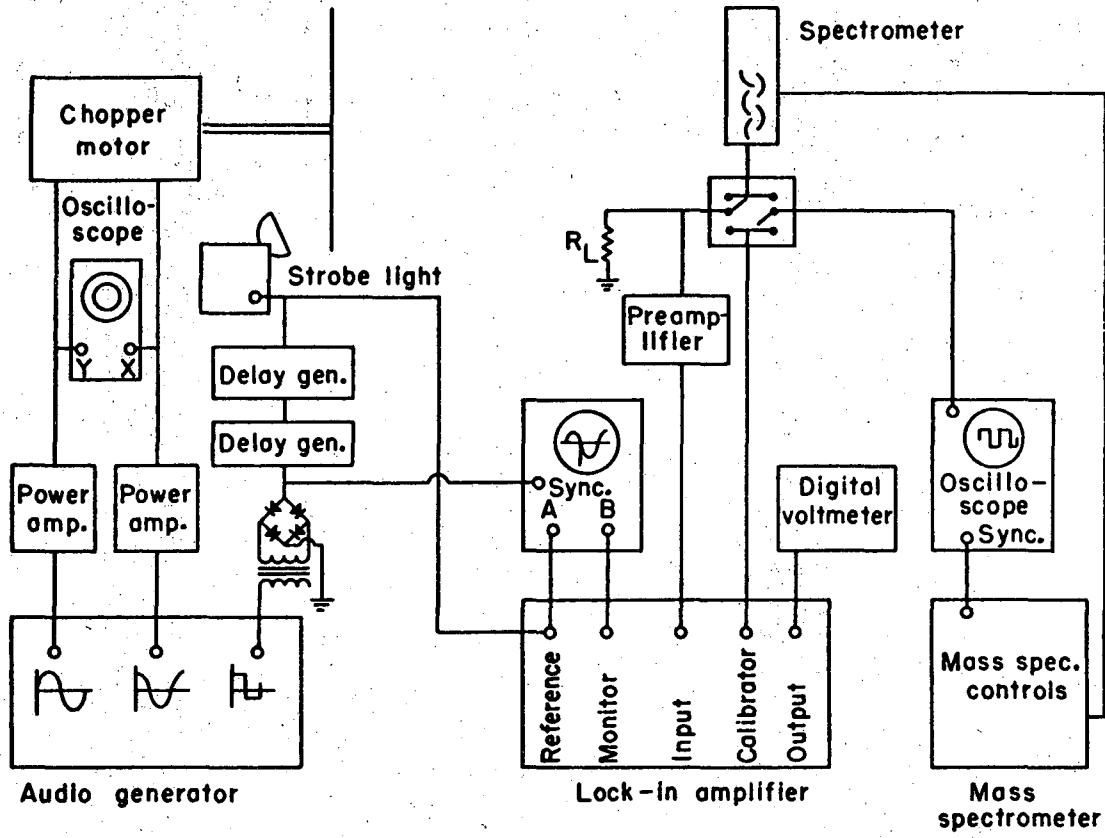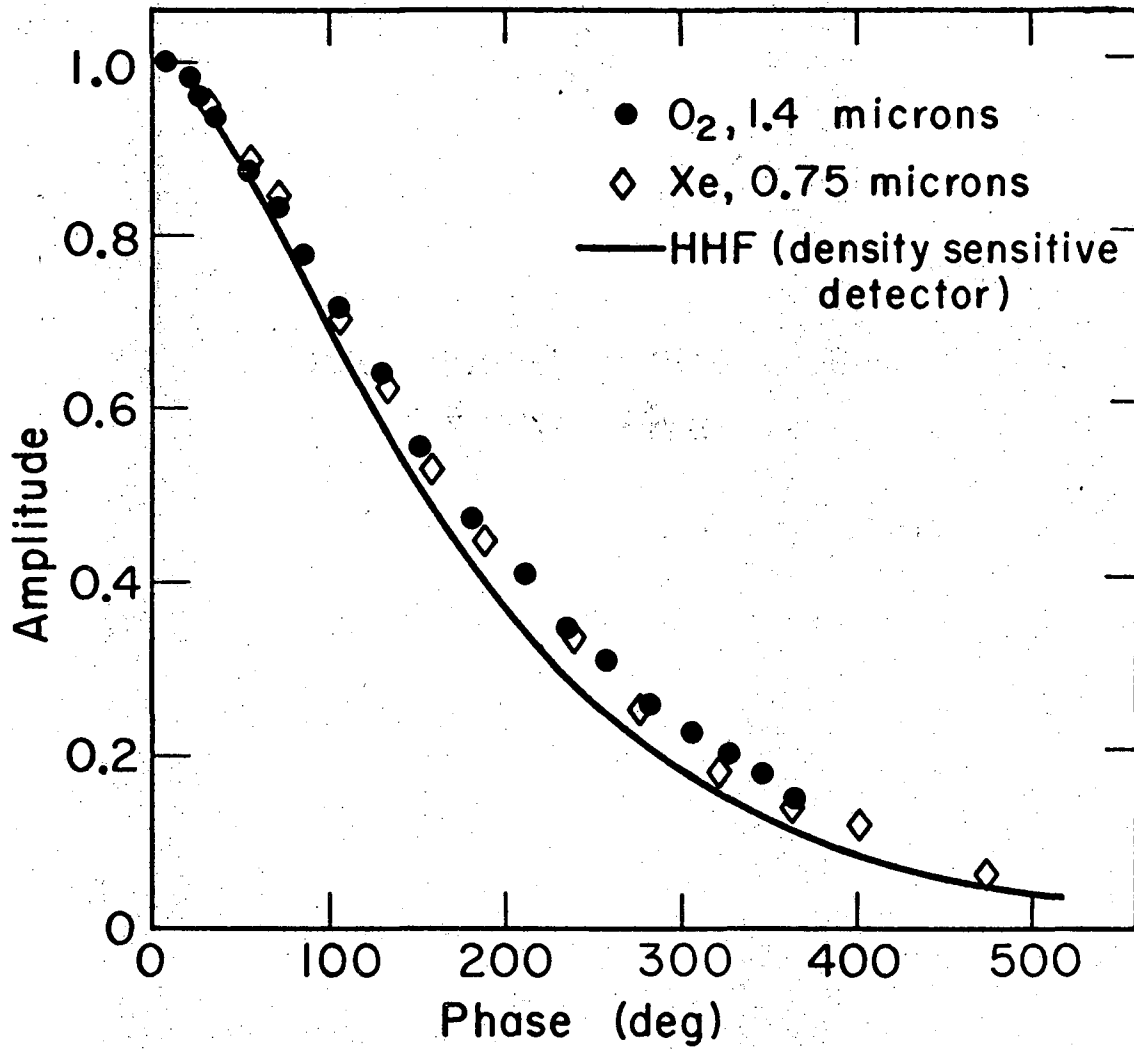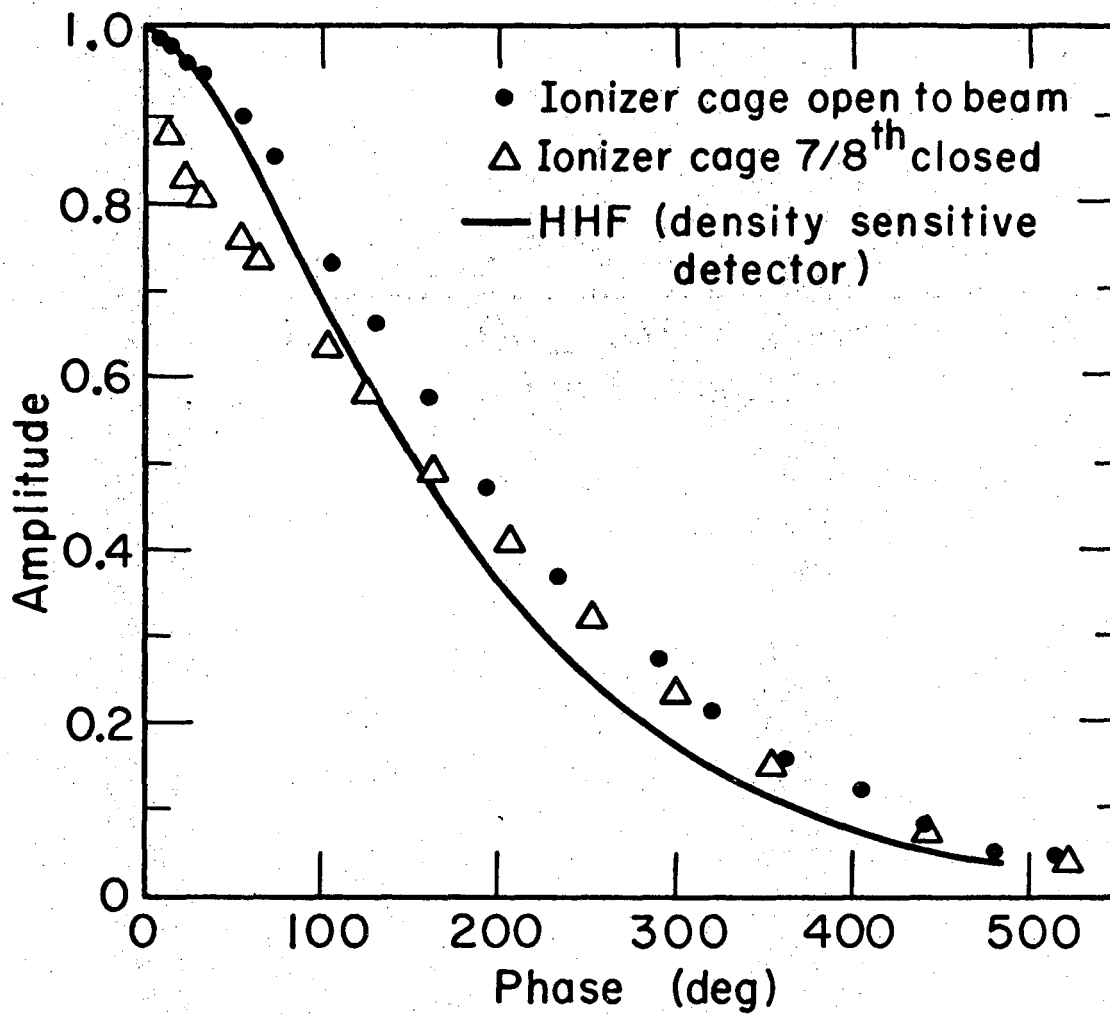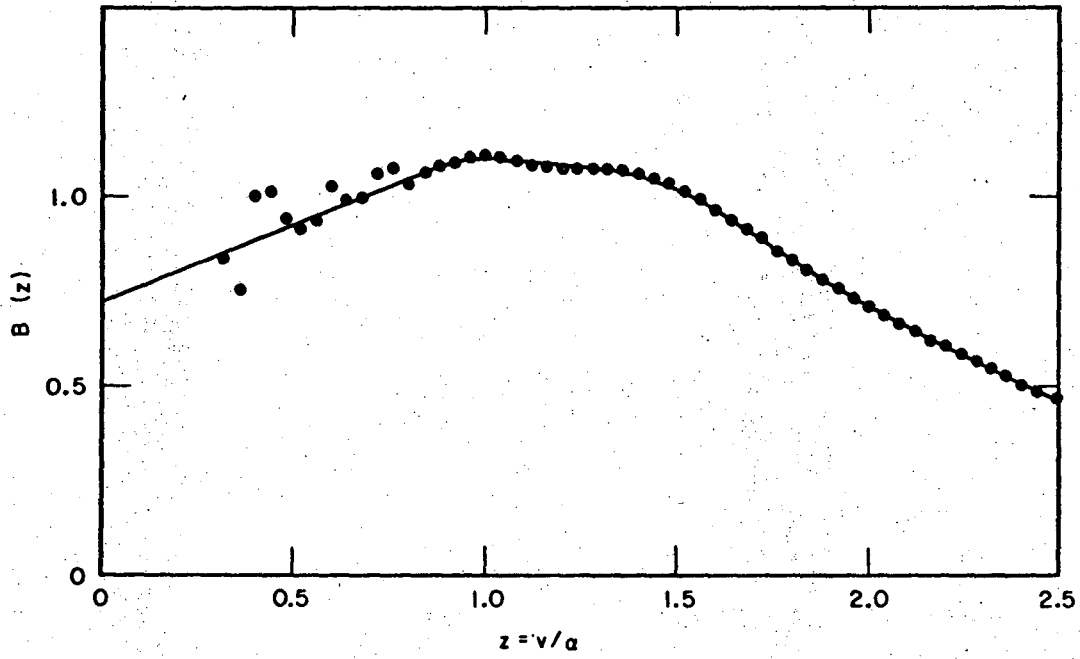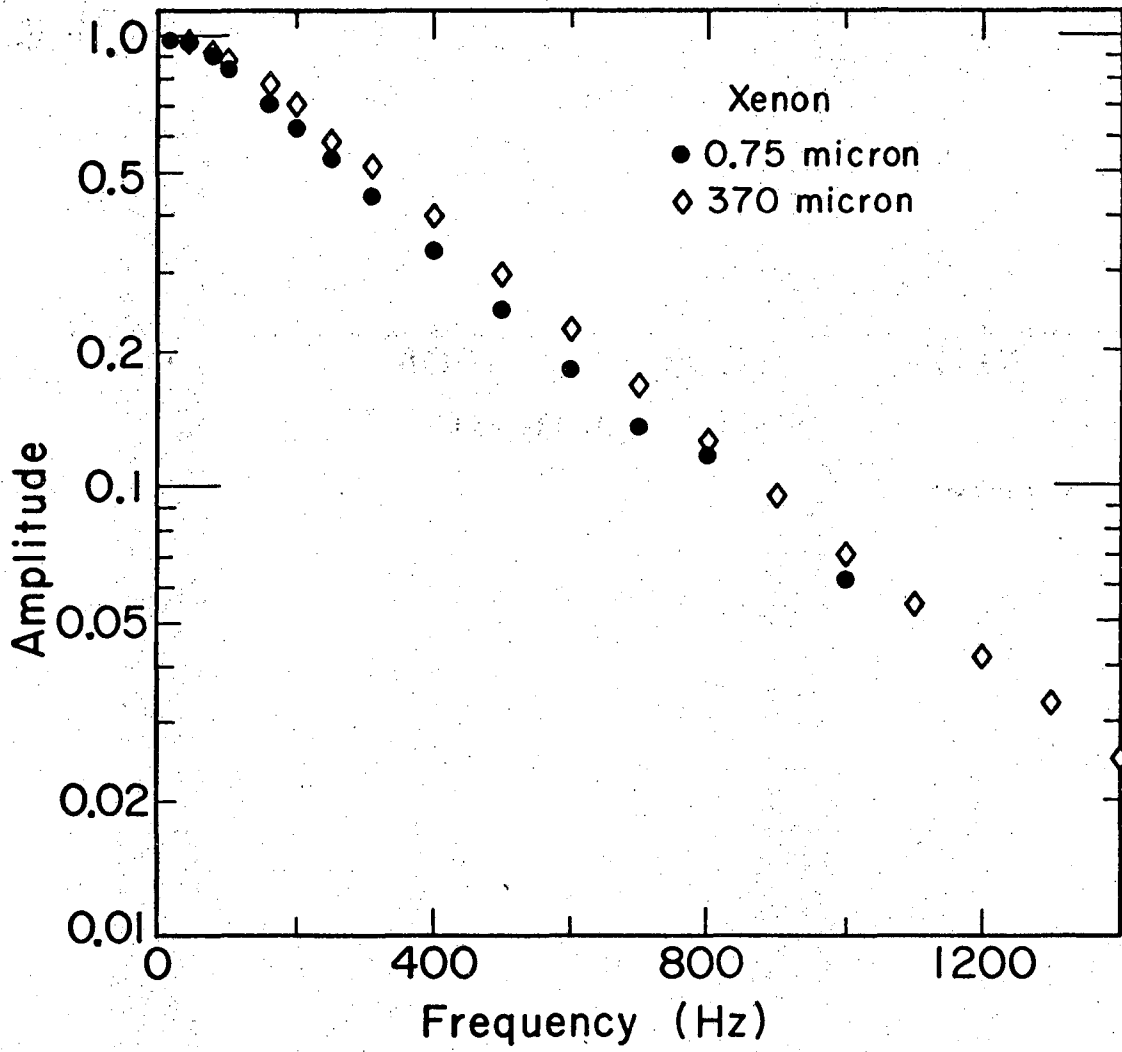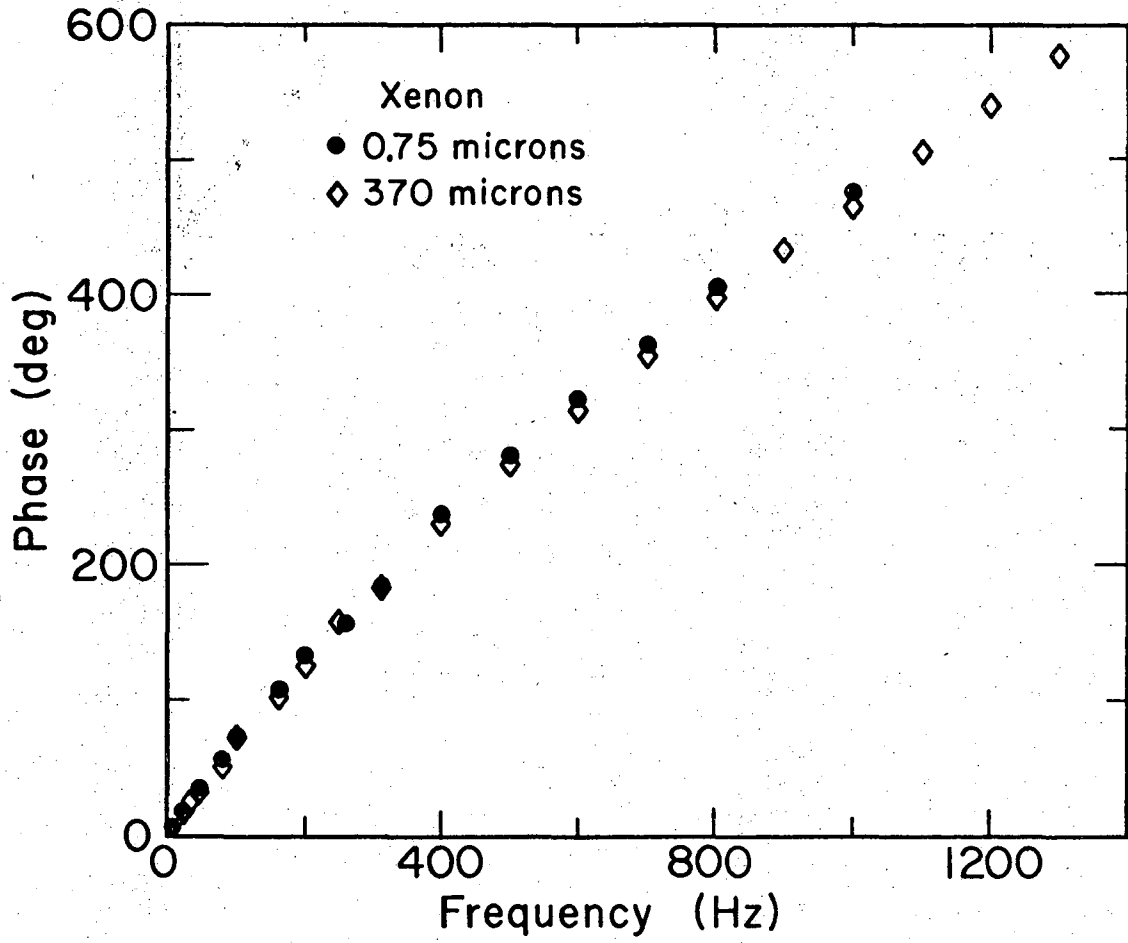
XBL6911-6131

XBL6911-6132
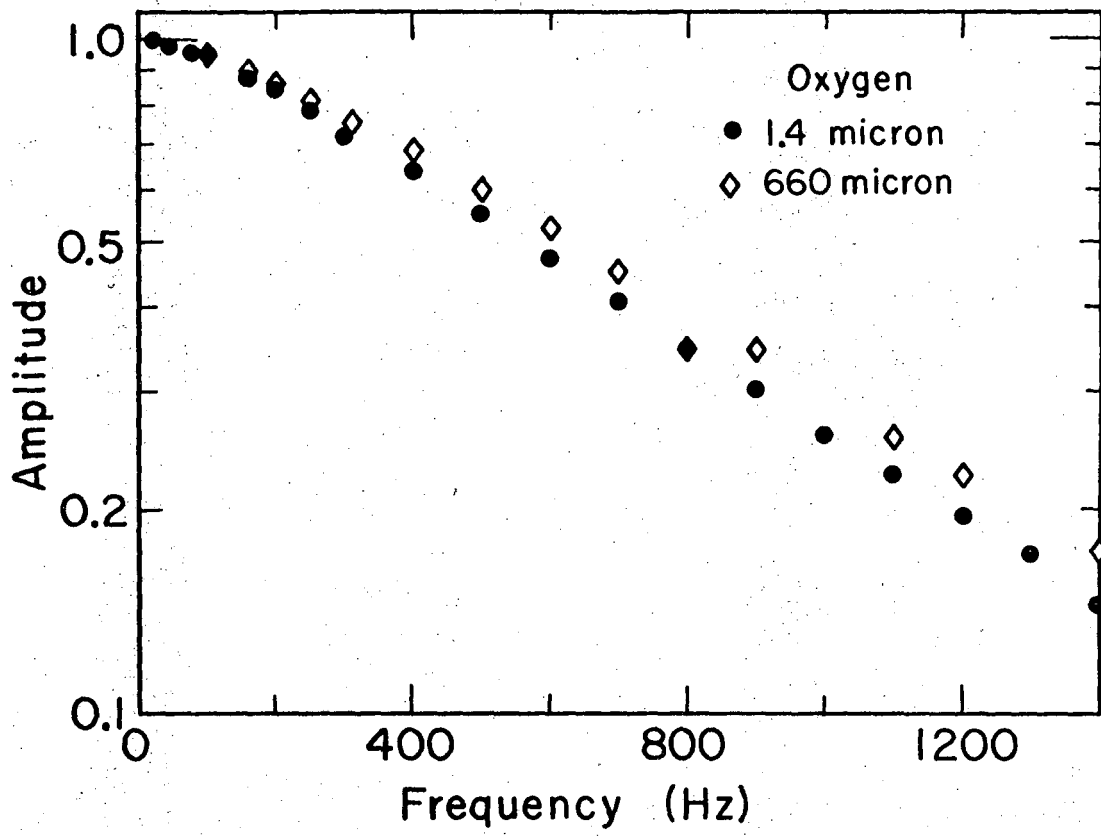
XBL6911-6130

XBL 6911-6129

Velocity distributions f(z)
- - - Maxwellian
——— Theoretical at $(Kn)^{-1} > 10$
• • • Measured, Xe at $(Kn)^{-1} = 52$
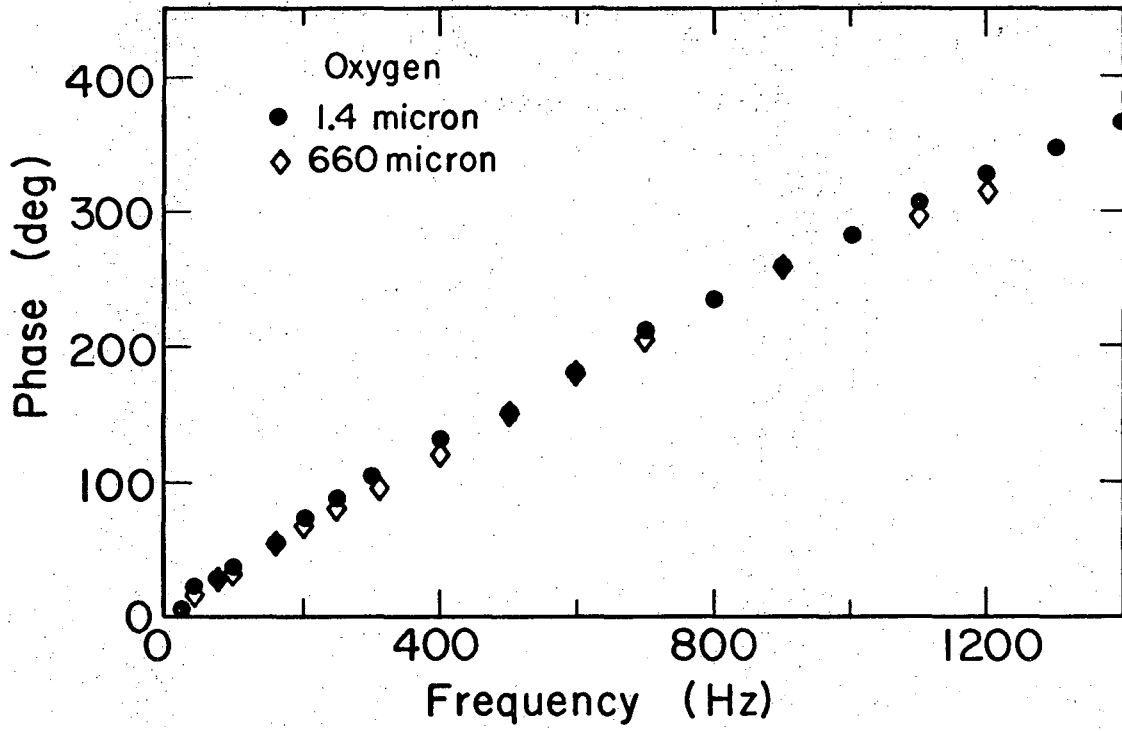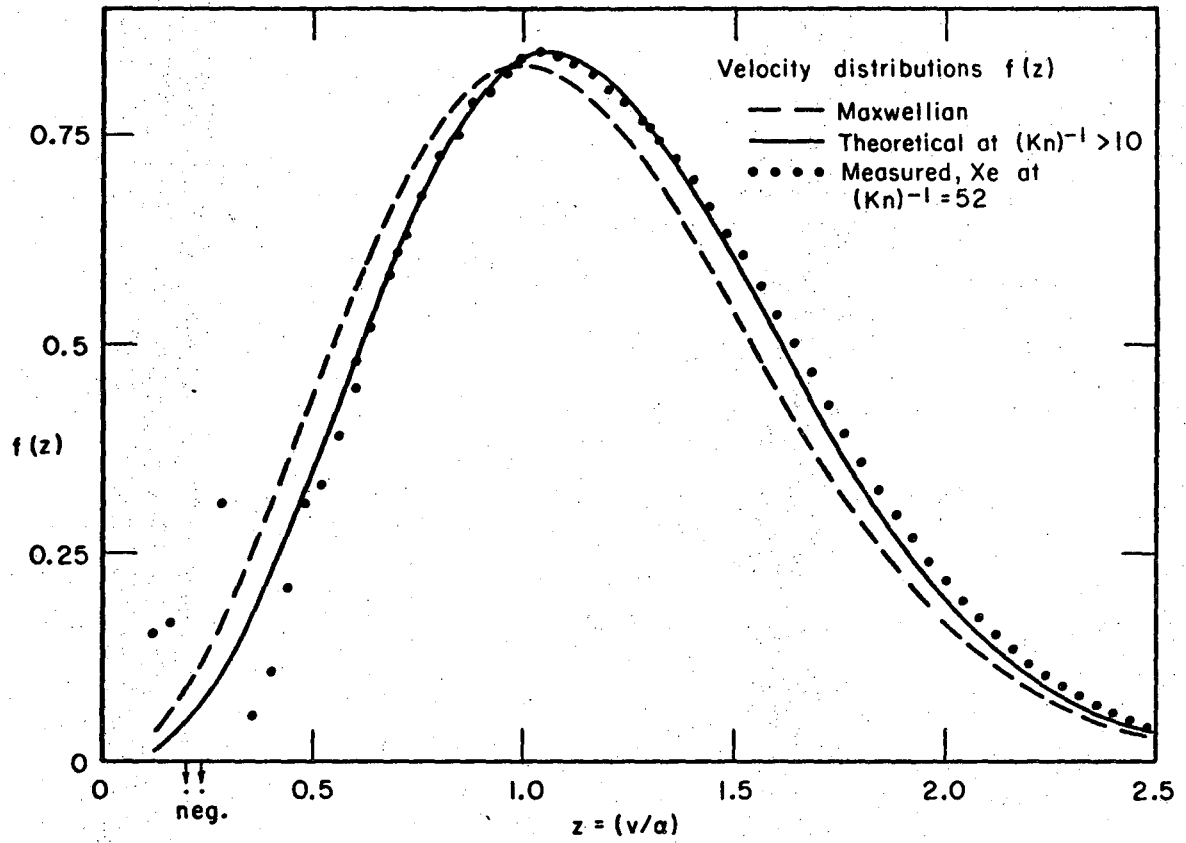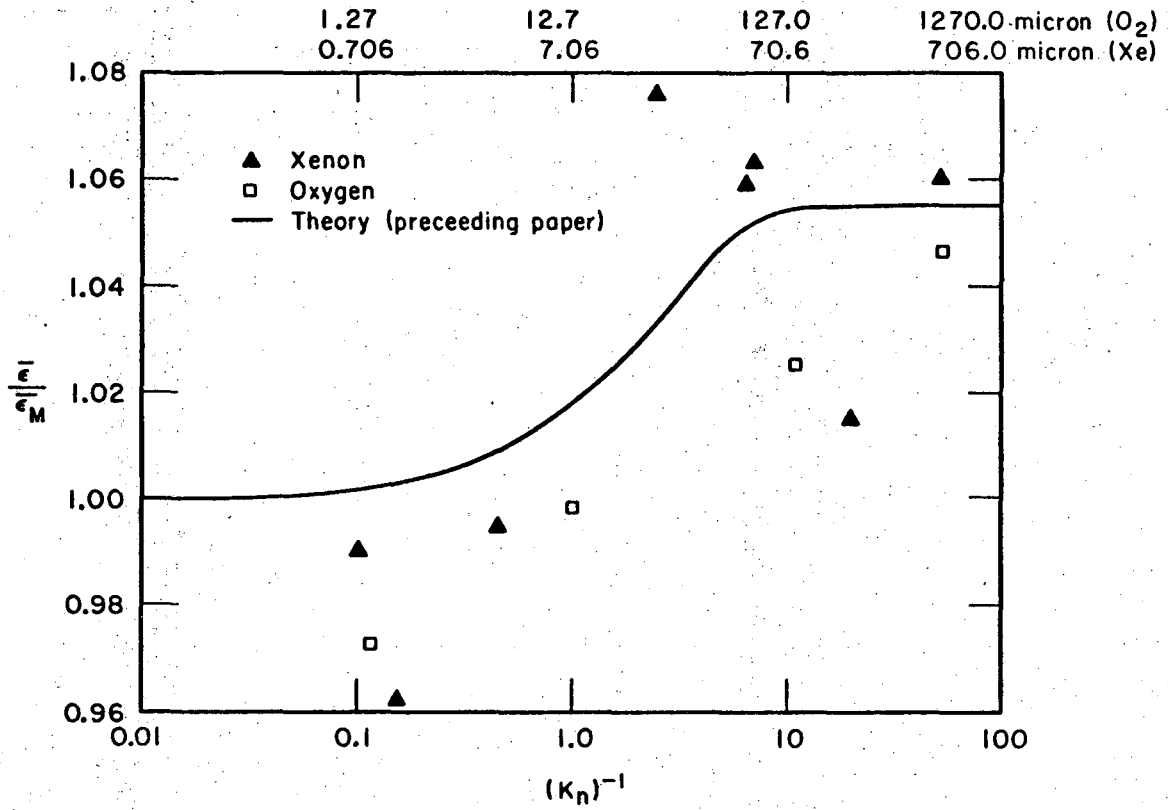
XBL6911-6161

XBL6911-6162

12
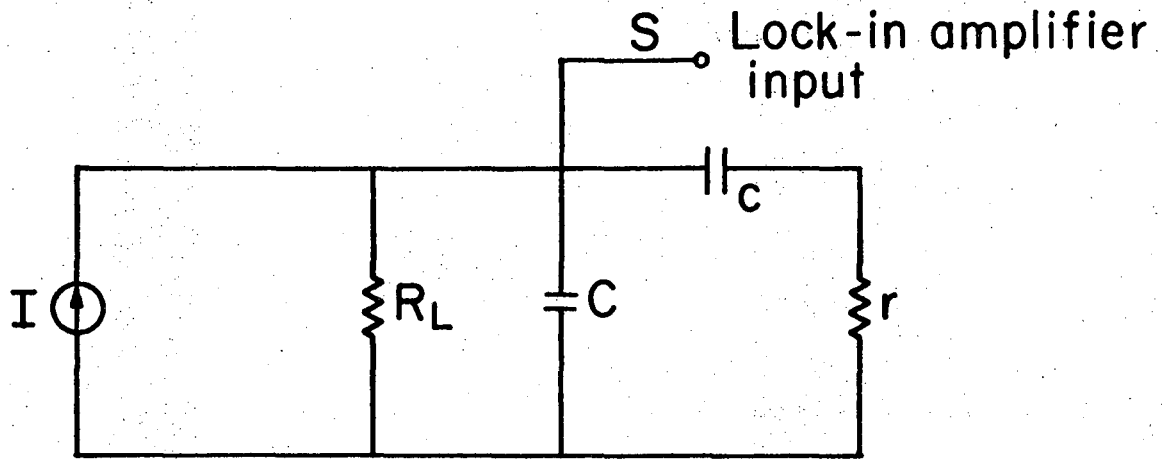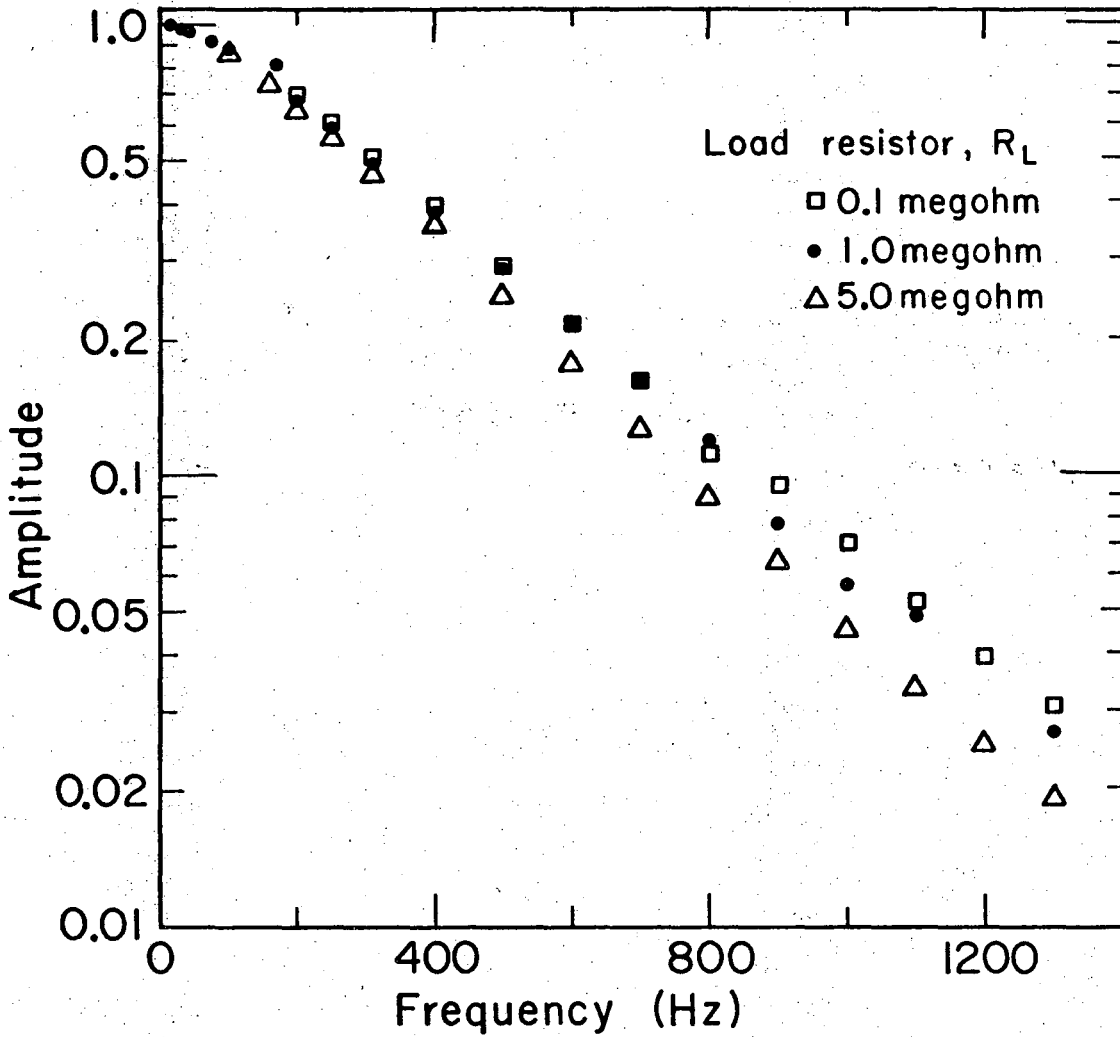
XBL6911-6142

XBL6911-6141
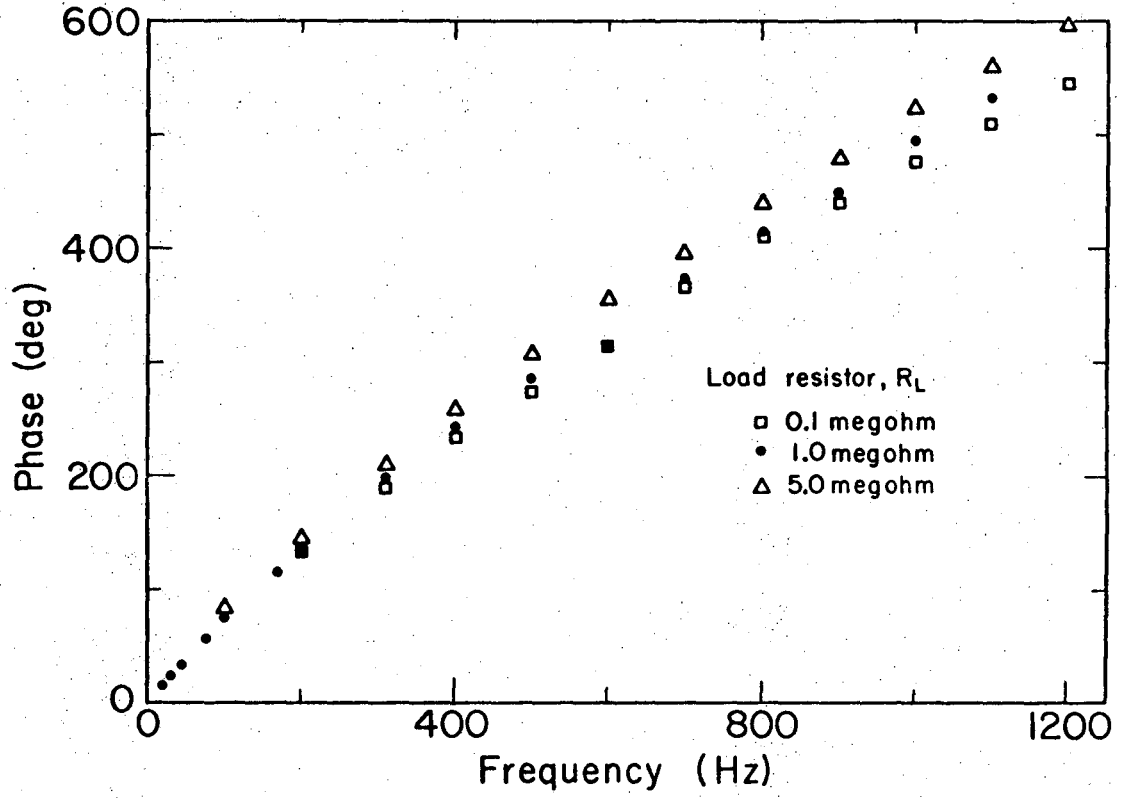
XBL6911-6140

XBL6911-6138

16
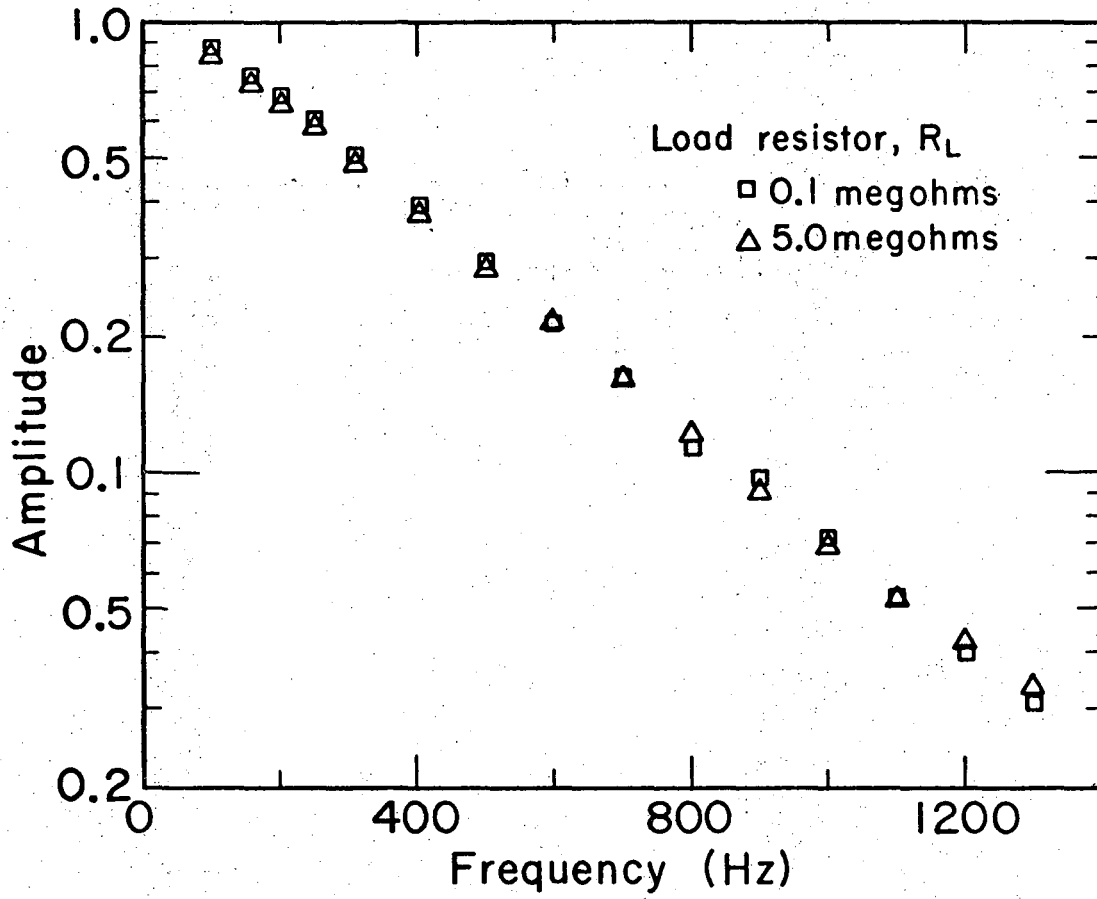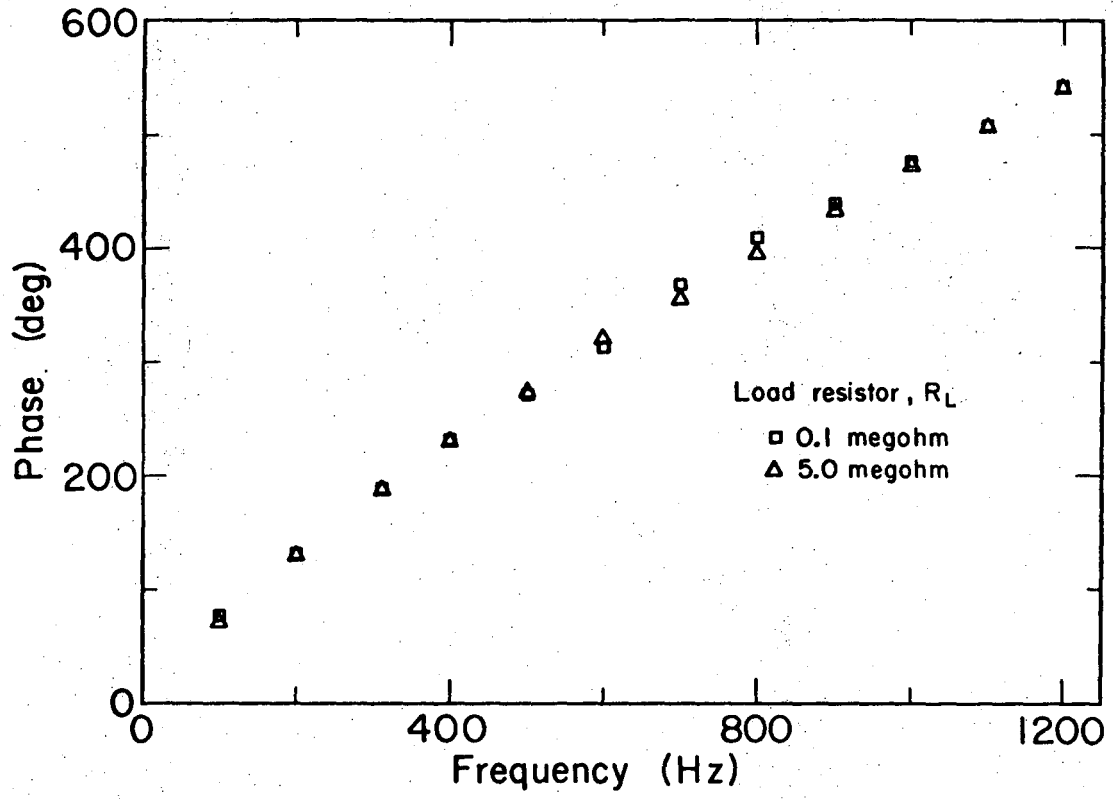
XBL6911-6139

XBL6911-6137